HYDRODYNAMICS OF INTERNAL SOLITONS AND A COMPARISON OF SIR-A AND SIR-B DATA WITH OCEAN MEASUREMENTS

J. R. Apel, R. F. Gasparovic and D. R. Thompson
The Johns Hopkins University
Applied Physics Laboratory
Laurel, Maryland

ABSTRACT

Large internal solitary waves have been observed by Shuttle SIR-A and SIR-B at locations in the Andaman Sea and the New York Bight. Satellite imagery and oceanographic measurements are used in conjunction with hydrodynamic interaction and electromagnetic scattering models to estimate the expected SAR image intensity modulations associated with the internal waves. There is reasonable agreement between the predicted and observed internal wave signatures.

I. ANDAMAN SEA SOLITONS

The Andaman Sea is located along the eastern side of the Indian Ocean between the Malay Peninsula and the Andaman and Nicobar Islands. It is a maritime regime containing internal solitary waves of extraordinary amplitude, wavelength and speed that exhibit signatures via surface roughness variations that are visible to the eye, to cameras, to scanning imagers, and to imaging radars. Internal solitary waves, or solitons, are generally waves of depression, more or less isolated from their fellows, that propagate over great distances with very little change in shape. Several satellite images have revealed that the Andaman Sea is rich in such excitations. The joint US-USSR space mission, Apollo-Soyuz, returned color photographs that showed narrow stripes of rough water in the sun glint region. These were interpreted by Apel (1979) as surface signatures of large internal waves, presumably produced by semidiurnal tidal flow over underwater topography; the inferred group speeds were approximately 2.5 m/s, as derived from their interpacket separation. In addition, examinations of visible wavelength imagery from the scanner on the Defense Meteorological Satellite Program (DMSP) spacecraft revealed similar surface signatures on several dates. Synthetic aperture radar images from the Shuttle Imaging Radar-A (SIR-A) on November 11, 1981, also contain several internal wave packets in the vicinity of the Andaman and Nicobar Islands (Cimino et al., 1982; Ford et al., 1983; Apel et al., 1986).

Figure 1 is a section of the SIR-A radar image of that date, having dimensions of 51.2 by 51.2 km, with the white marks along the lower border being 1-s time tics (or a distance of 7.14 km). North is along the direction shown, at an angle of approximately 38° from the lower edge. It is a high resolution (40-m), geographically corrected representation of the surface wave roughness variations and has been selected for further analysis because of the qualities that the internal waves possess. The objectives of the analysis are: (a) to use the historical density data in conjunction with the known nonlinear properties of internal solitons to estimate the amplitudes, currents, strain

rates, and propagation speeds from the SIR-A image; (b) to estimate wind speed and direction from the image; and (c) to apply theories of radar backscatter modulation to the deduced hydrodynamic and wind properties, in order to calculate the radar signatures. The signatures will then be compared with image intensity modulations.

The internal solitons are revealed mostly by dark (smooth) regions, with the associated rough regions not clearly visible, probably due to the large, 43° earth-incidence angle of the synthetic aperture radar. The approximately semicircular dark region near right center is thought to be an area of rainfall toward which the local winds are blowing, as revealed by subtle wind row streaks overlying portions of the waves; the wind direction is nearly from the west. The wind speed is estimated to be about 3 to 4 m/s, based on the general level of backscatter and the visibility of the waves, but the error in this estimate is easily ±100 percent.

The hydrodynamic properties are estimated from the image and from the historical density data by the application of a "modulated cnoidal wave" model of the solitary waves (Apel and Gonzales, 1983). In the Korteweg-deVries equation describing such solitons, a Mode-1 solitary wave train can be written as the product of an eigen function, W(z), giving the relative amplitude variation with depth, z, and a horizontal amplitude function, A(s,t), describing propagation along a horizontal arc, s(x,y), in the x,y plane. Thus, we write for the amplitude, η,

$$\eta(x,y,z,t) = W(z)\, A(x,y,t)\,. \tag{1}$$

The equations obeyed by the separation functions W and A are

$$\frac{d^2W}{dz^2} + k_t^2 \left[\frac{N^2(z)}{\omega^2} - 1\right] W = 0\,,$$

$$W(0) = W(-H) = 0\,, \tag{2}$$

(where the ocean bottom is at the depth -H), and the K-dV equation,

$$\frac{\partial A}{\partial t} + c_0 \left(\frac{\partial A}{\partial s} + \gamma \frac{\partial^3 A}{\partial s^3} + \alpha A \frac{\partial A}{\partial s}\right) = 0\,. \tag{3}$$

Here, $\omega = \omega(k_\ell)$ is the dispersion equation relating wave angular frequency, ω, to linear wave number, k_ℓ; the quantities, N, γ, and α are environmental parameters termed the Brunt-Väisälä (or buoyancy) frequency, the dispersion coefficient, and the nonlinear coefficient, respectively. These may all be calculated from a knowledge of the variation of density with depth.

A useful approximate solution to the K-dV equation describing a bounded wave packet may be written as a modulated cnoidal function, wherein a propagating envelope function, $\eta_0(s-ct)$, moving at speed, c, is assumed to multiply the periodic cnoid, just as a modulated cosine may be used to describe a propagating linear wave packet. In this fashion, the varying amplitudes and degrees of nonlinearity existing within a group of waves such as those in Fig. 1 may be modeled without invoking the full apparatus of inverse scattering theory in the analysis. Algebraic relationships exist between the stretched wavelength, λ_s, and k_ℓ, m, η_0, and c, and can be used to estimate the amplitude and speed if the other quantities can be evaluated. These relationships are

$$\lambda_s = \left(\frac{2\pi}{k_t}\right) \cdot \frac{K(m)}{\pi/2} = \lambda_\infty \frac{K(m)}{\pi/2} , \tag{4}$$

$$m = \frac{\alpha\eta_0}{\frac{1}{2}\gamma k_t^2} = \frac{\alpha\eta_0}{c - c_0} , \tag{5}$$

$$\begin{aligned} c &\approx c_0 \left(1 - \tfrac{1}{2}\gamma k_t^2 + \frac{\alpha\eta_0}{3}\right) \\ &\approx c_t + c_0 \frac{\alpha\eta_0}{3} . \end{aligned} \tag{6}$$

In Eq. 4, $\lambda_\infty = 2\pi/k_\ell$ is the small-amplitude, linear wavelength and K(m) is the complete elliptic integral of the first kind, which for m=0 reduces to $\pi/2$, while for $m \to 1$, $K(m) \to \infty$. In Eq. 6, the speed c is given in terms of the long-wavelength speed c_0 for which $k_\ell \approx 0$. The speed of a solitary wave is increased by the nonlinear amplitude-dependent term in Eq. 6; thus, larger solitons travel faster than smaller ones, all else being equal.

Using these quantities, the modulated cnoidal wave solution can be written as

$$\begin{aligned} \eta(x,y,z,t) &= -W(z)\eta_0(s - ct) \\ &\times cn_m^2 \left[\tfrac{1}{2}(\mathbf{k}_t \cdot \mathbf{s} - \omega t + \Phi)\right] . \end{aligned} \tag{7}$$

To apply Eqs. 4 to 7 to the case at hand, the image of Fig. 1 is used to evaluate (a) λ_∞ from the wavelength at the rear of the wave packet, and (b) the stretched wavelength, λ_s, from the spacings of the other waves throughout the packet. The ratio λ_s/λ_∞ is used to calculate the values of K(m) and m from Eq. 4; from Eq. 5 one then derives η_0.

Having obtained the wave amplitudes, the known hydrodynamics of the waves may be used to obtain the currents, u and w, and the horizontal strain rate, $\partial u/\partial s$, as well as the other desired properties.

In order to evaluate the equations numerically, functional forms of W(z) and its derivative are required; these are obtained via numerical solutions to Eq. 2. This in turn requires a vertical profile of $N^2(z)$ in terms of water density, ρ:

$$N^2(z) = -\frac{g}{\rho}\cdot\frac{d\rho}{dz} \quad . \tag{8}$$

A temperature profile was obtained from Osborne et al. for the Andaman Sea (Osborne and Burch, 1980) and used in this calculation.

Figure 2 illustrates the estimated surface current and surface strain rates versus distance, s - ct, throughout approximately 40 km of the packet. The peak currents are about 1.1 m/s, the strain rates are 1.3 x 10^{-3} s^{-1} and peak amplitudes (not shown) are approximately 60 m - reasonable values in light of the measurements made in the Andaman to date (Osborne and Burch, 1980).

Figure 3 shows a comparison between the measured intensity modulation along the cut through the SIR-A image of Fig. 1 and the predicted modulation from our wave-current interaction model. One can see that the predicted modulation depth agrees fairly well with that measured from the synthetic aperture radar image. The intensity minima occur at nearly the same position and the spatial behavior of the predicted and measured curves is in reasonable agreement, although the theory underestimates the observations by about a factor of two.

II. NEW YORK BIGHT

During Orbit 91 (11 October 1984) of the SIR-B mission on the shuttle Challenger, a synthetic aperture radar image of oceanic internal waves was obtained simultaneously with ship and current-meter measurements of the waves. These observations were part of the second phase of the Synthetic Aperture Radar Signature Experiment (SARSEX), a major experiment sponsored by the Office of Naval Research to investigate the basic hydrodynamic and electromagnetic phenomena responsible for internal wave signatures in SAR images and to test theories for predicting such signatures. The SIR-B image taken at 05:03:08 EDT (Fig. 4) shows several packets of tidally generated internal waves, low to moderate wind fronts, and the location of the research vessel Cape. The geographical area extends from about 100 km south of Long Island to immediately northeast of the Hudson Canyon, near 40°N, 72°15'W, a region that had been studied by Apel and coworkers (Apel et al., 1975a,b) during observational programs on internal waves on the continental shelf.

In situ measurements were made of horizontal water velocity components from current meters at depths of 15 and 67 m, water column temperature and density profiles, 200-kHz downward-looking echo sounder internal wave profiles, surface wave height spectra, and wind speed. The major properties of the internal wave field can be estimated when these measurements are used in conjunction with the type of internal wave model used above, with certain modifications. From the in situ measurements and a solution of the internal

wave equation, we find that $\eta_0 \simeq 9$ m, L $\simeq$ 250 m, and c $\simeq$ 0.4 m/s. At the surface, the estimated maximum induced current is $u_0 \simeq 0.15$ m/s, and the maximum surface current gradient, or strain rate, is approximately 0.004 s^{-1} (Gasparovic et al., 1986).

A more extensive observational program of some nonlinear internal waves was carried out four weeks earlier during Phase I of SARSEX. This effort was structured to quantify the dominant processes contributing to the SAR signatures of internal waves: (i) the internal wave hydrodynamics, especially the surface current strain rates; (ii) modifications to the surface wave spectrum induced by the currents; (iii) the radar backscatter from the modulated surface waves; and (iv) the formation of SAR images from the backscatter modulations (Gasparovic et al., 1985).

A theory describing the perturbation of the surface wave height spectrum by the internal wave surface currents has been used to calculate the expected backscatter modulations associated with the internal waves (Hughes, 1978). This theory assumes that the energy input from the wind acts to restore the surface wave height spectrum S(k, x , t), which is perturbed by the presence of the internal wave currents u(x,t), to its equilibrium value $S_0(k)$. In particular, it is assumed that the fractional change in the wave action spectrum

$$N(\mathbf{k}, \mathbf{x}, t) = \rho \frac{\omega}{k} S(\mathbf{k}, \mathbf{x}, t) \tag{9}$$

(where ρ is the water density) is proportional to the departure of the spectrum from its equilibrium value $N_0(k)$. Mathematically, this implies

$$\begin{aligned} \frac{1}{N}\frac{dN}{dt} &= \frac{1}{N}\left(\frac{\partial N}{\partial t} + \dot{\mathbf{x}} \cdot \nabla_x N + \dot{\mathbf{k}} \cdot \nabla_k N\right) \\ &= -\frac{\beta(\mathbf{k})}{N_0}(N - N_0) \end{aligned} \tag{10}$$

where

$$\dot{x}_i = \frac{\partial \omega}{\partial k_i} + u_i \tag{11}$$

and

$$\dot{k}_i = -k_j \frac{\partial u_j}{\partial x_i} \tag{12}$$

In these equations, the indices i, j = 1, 2 denote horizontal coordinates, and repeated indices are summed. The function $\beta(k)$ - the so-called wave relaxation rate - determines the effectiveness of both wind and dissipation in restoring equilibrium (Hughes, 1978). There is at present considerable uncertainty about its exact functional form, although there is general agreement that it increases with wave number and wind speed. We made the calculations that follow by using Hughes' expression for $\beta(k)$ which is consistent with field observations.

To relate the internal wave-induced change in surface wave spectrum to the SAR image intensity modulation, we make use of the fact that ocean backscatter at the SIR-B radar wavelength λ_0 = 23.5 cm and incidence angle θ is dominated by Bragg scattering (Thompson and Gasparovic, 1986; Thompson, 1986). In this limit, the normalized radar cross section σ is proportional to the surface wave spectrum of the Bragg waves, that is, those waves traveling in the radar "look" direction with a wavelength $\lambda_B = \lambda_0/2(\sin\theta)$. The fractional change in cross section from its mean value σ_0 is given by

$$\frac{\Delta\sigma}{\sigma_0} = \frac{N(\mathbf{k}_B, x, t) - N_0(\mathbf{k}_B)}{N_0(\mathbf{k}_B)} \tag{13}$$

where k_B is the Bragg wave number. When the internal wave features propagate in the radar look direction as in Fig. 4, the SAR image intensity variations are essentially equivalent to the cross-sectional variations given by Eq. 13.

Image intensity variations for some of the features of the internal waves in Fig. 4 are shown in Fig. 5, which was taken through the wave group along the vertical line A-A'; it shows nine distinct waves in the packet with peak-to-peak intensity variations ranging from 2 to 12 dB. The average spacing between waves in this packet is approximately 380 m. There is another group of waves near the center of the image along the vertical line B-B' and the four waves at the front of this packet have peak-to-peak intensity variations of 3 to 10 dB.

We have made predictions of the SAR image intensity modulations for these internal waves using the above theory, with internal wave and surface parameters obtained from the in situ observations. Maximum internal wave surface strain rates of 0.002 to 0.005 s^{-1} were assumed, consistent with intrapacket variations encountered during the Phase I observations. The large-scale brightness variations in Fig. 4 are indicative of the presence of wind speeds greater than the value 1 m/s recorded at the ship location which is in a dark region of the image. For the wave packet along A-A', we assumed a wind speed of 2 m/s along line B-B'; the actual wind speed is presumed to lie between these two values. With a wind speed of 2 m/s, the calculated peak-to-peak SAR image intensity modulations range from 2 to 7 dB for maximum surface strain rates of 0.002 and 0.005 s^{-1}, respectively. These calculated modulations agree with the observations along lines A-A' and B-B' to within 3 to 5 dB, or within a factor of 2 to 3. This result is consistent with initial findings for the Phase I SAR aircraft L-band images, for which more extensive comparisons between theory and observations are possible.

ACKNOWLEDGEMENTS

The authors appreciate the SIR-A and SIR-B data support by the Jet Propulsion Laboratory. This work was supported by U.S. Naval Sea Systems Command under Contract N00024-56-C-5301.

REFERENCES

J. R. Apel, H. M. Byrne, J. R. Proni, and R. L. Charnell, J. Geophys. Res. 80, 865 (1975).

J. R. Apel, J. R. Proni, H. M. Byrne, and R. L. Sellers, Geophys. Res. Lett. 2, 128 (1975).

J. R. Apel, "Observations of Internal Wave Surface Signatures in ASTP Photographs," Apollo-Soyuz Test Project II, F. El-Baz and D. M. Warner, eds. NASA SP-412 (1979).

J. R. Apel and F. I. Gonzalez, J. Geophys. Res. 88, 4459 (1983).

J. R. Apel, D. R. Thompson, D. G. Tilley, and P. Van Dyke, "Hydrodynamics and Radar Signatures of Internal Solitons in the Andaman Sea," Johns Hopkins APL Technical Diget, 6, 330 (1986).

J. B. Cimino and C. Elachi, "Shuttle Imaging Radar-A (SIR-A) Experiment," NASA/JPL 82-77, pp. 5-53 (1982).

J. P. Ford, J. B. Cimino, and C. Elachi, "Space Shuttle Columbia Views the World with Imaging Radar: The SIR-A Experiment," NASA/JPL 82-95, pp. 144-145 (1983).

R. F. Gasparovic, J. R. Apel, D. R. Thompson, and J. S. Tochko, "A Comparison of SIR-B Synthetic Aperture Radar Data with Ocean Internal Wave Measurements," Science, 232, 1529 (1986).

B. A. Hughes, J. Geophys. Res. 83, 455 (1978).

A. R. Osborne and T. L. Burch, "Internal Solitons in the Andaman Sea," Science 208, 451 (1980).

SARSEX Experiment Team, "SARSEX Interim Report" (Report STD-R-1200, Johns Hopkins University Applied Physics Laboratory, Laurel, MD, May 1985).

D. R. Thompson and R. F. Gasparovic, Nature (London) 320, 345 (1986).

D. R. Thompson, "Intensity Modulations in Synthetic Aperture Radar Images of Ocean Surface Currents and the Wave/Current Interaction Process," Johns Hopkins APL Technical Digest, 6, 346 (1986).

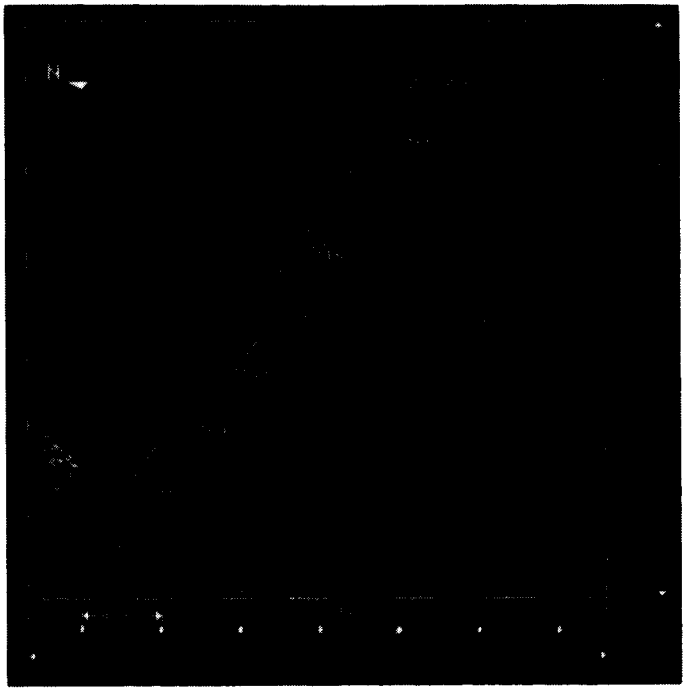

Figure 1. L-band radar image from SIR-A taken November 11, 1981, near the Andaman Islands, showing a packet of 6-kilometer-long solitons and what is thought to be a rain squall. Dimensions are 51.2 by 51.2 kilometers.

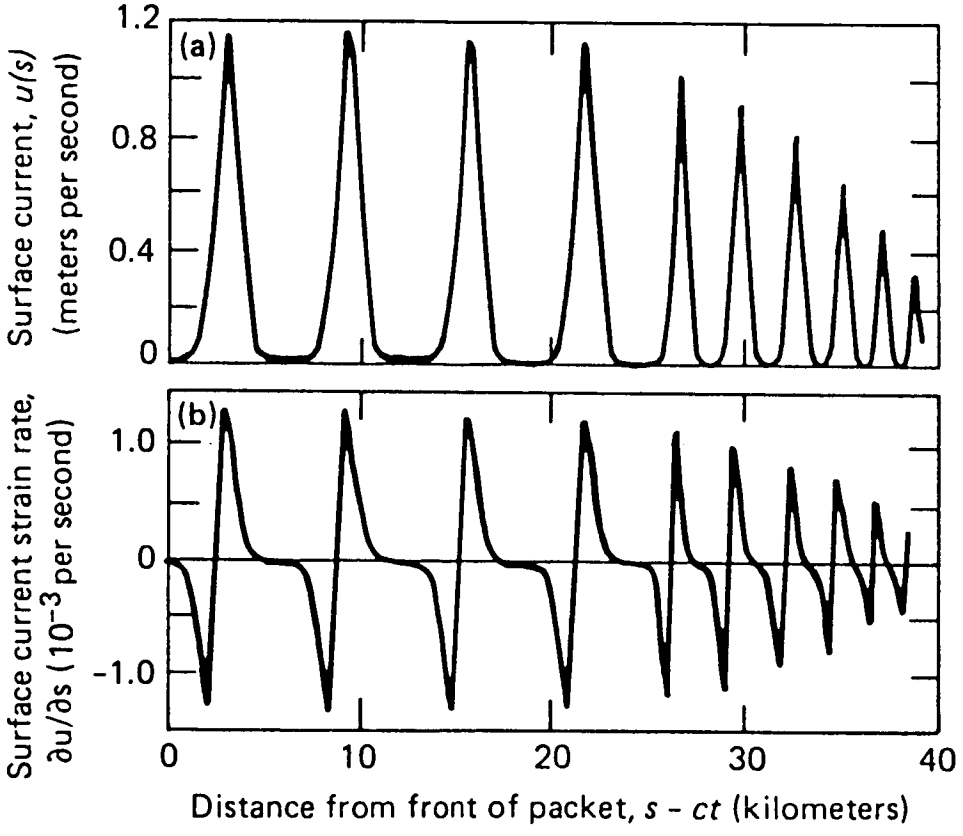

Figure 2. (a) Calculated horizontal surface currents and (b) surface strain rates for cnoidal wave packet. The front of the packet is at left.

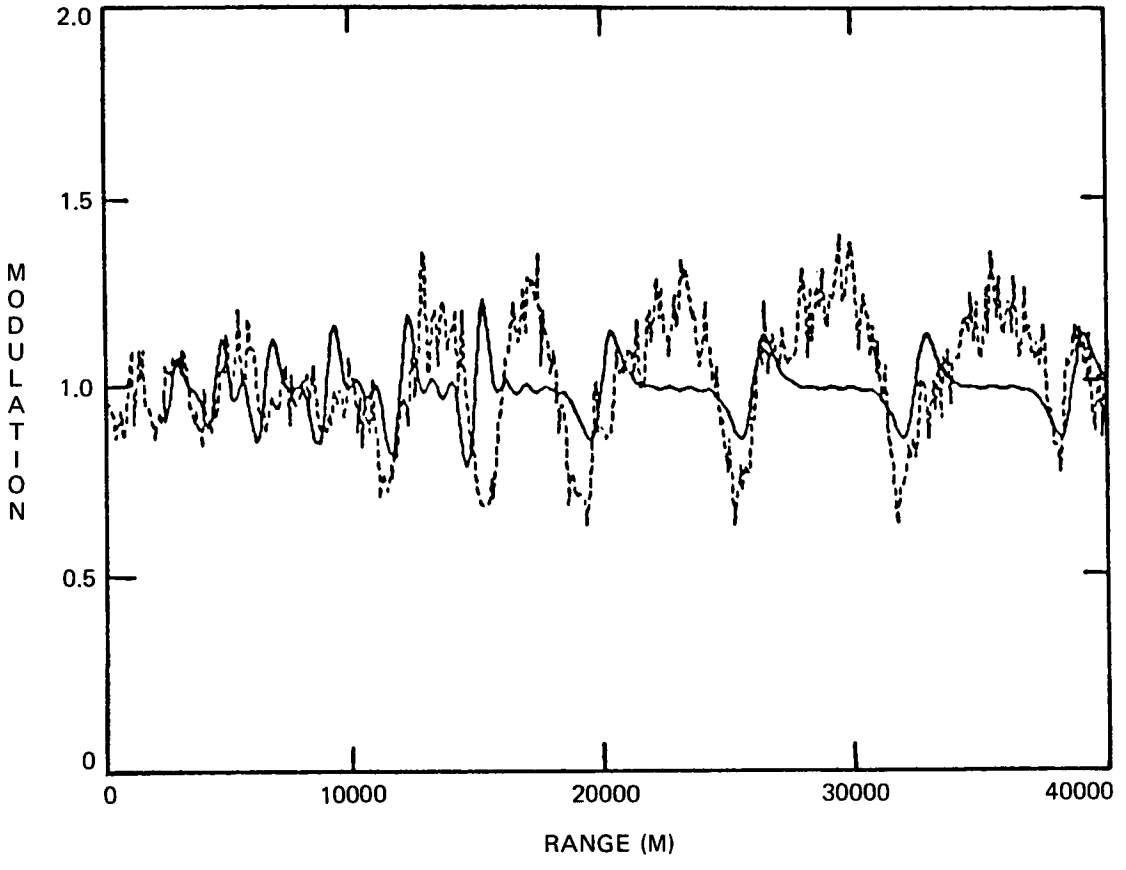

Figure 3. Comparison of observed (dashed curve) and calculated (solid curve) radar backscatter power modulation from rectangle of Fig. 1. The phase of the calculated modulation is reproduced quite well, but the amplitudes are generally underestimated by factors of 2 or more. The overall agreement is considered reasonable.

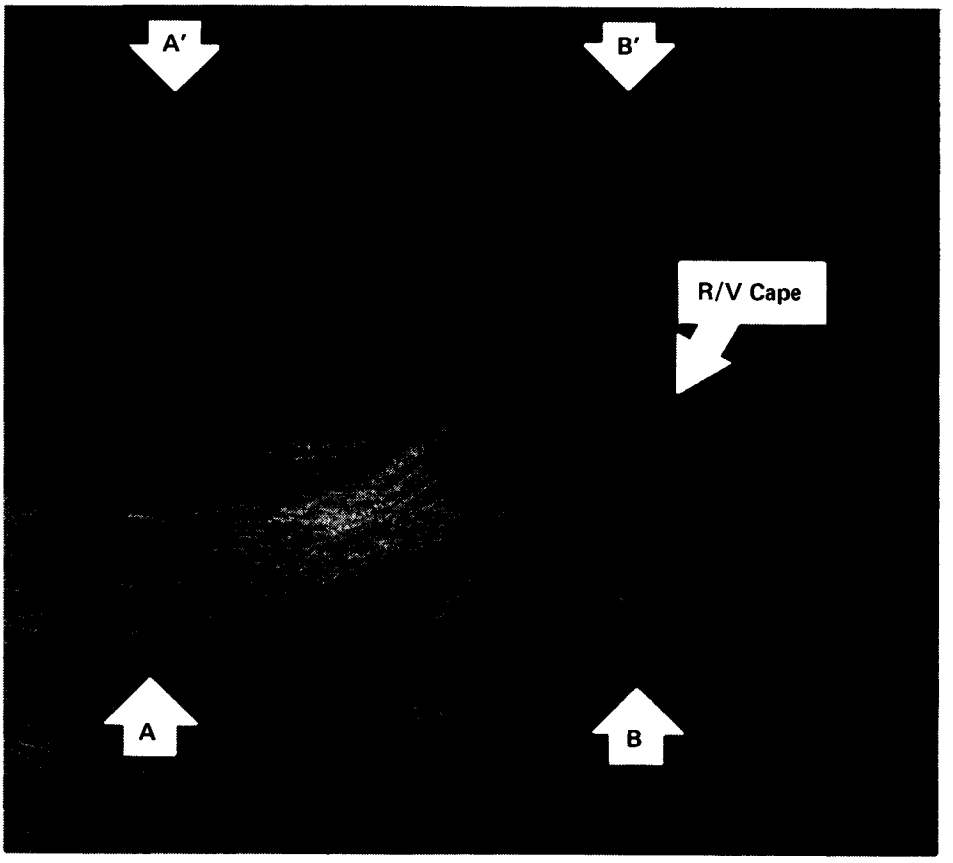

Figure 4. SAR image of oceanic internal wave features from orbit 96 of the SIR-B mission. The bright linear features crossing lines A-A' and B-B' are due to increased surface wave roughness within the internal wave packets, which are propagating toward the top of the image (313° true heading). A surface wind of 1 ms^{-1}, blowing toward 190° true heading, was recorded at the ship position. The radar incidence angle at the center of the image is 20°.

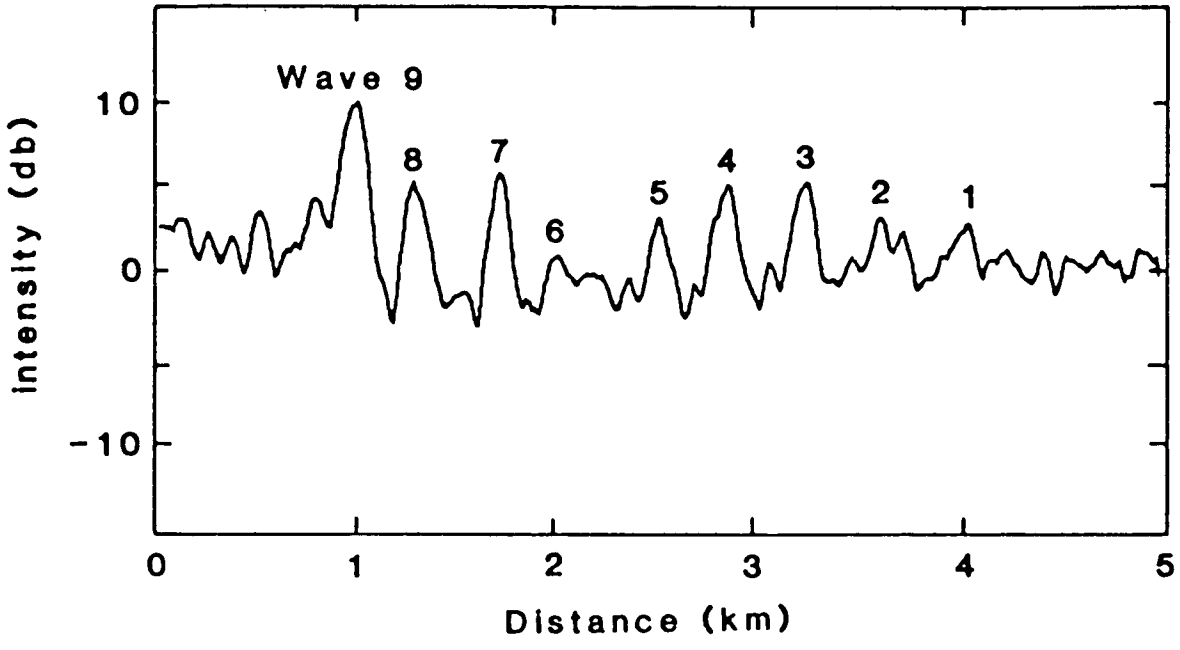

Figure 5. SAR image intensity traces through Fig. 4 along line A-A'. Trace has been averaged over 625 m in the azimuth direction and then smoothed 62.5 m in the range direction.